Preprint Cambridge Centre for Computational Chemical Engineering ISSN 1473 – 4273

On the Coagulation Efficiency of Carbonaceous Nanoparticles

Dingyu Hou[1,2], Diyuan Zong[3], Casper S. Lindberg[4], Markus Kraft[4,5,6], Xiaoqing You[1,2]

released: 16 September 2019

[1] Center for Combustion Energy
Tsinghua University
Beijing, 100084
China

[2] Key Laboratory for Thermal Science and Power Engineering of the Ministry of Education
Tsinghua University
Beijing, 100084
China

[3] China Shipbuilding New Power Co., Ltd
Beijing, 100097
China

[4] Department of Chemical Engineering and Biotechnology
University of Cambridge
Philippa Fawcett Drive
Cambridge, CB3 0AS
United Kingdom

E-mail: mk306@cam.ac.uk

[5] CARES
Cambridge Centre for Advanced Research and Education in Singapore
1 Create Way
CREATE Tower, #05-05
Singapore, 138602

[6] School of Chemical and Biomedical Engineering
Nanyang Technological University
62 Nanyang Drive
Singapore, 637459

Preprint No. 239

UNIVERSITY OF CAMBRIDGE

Keywords: Coagulation efficiency, nascent soot, potential well depth, carbonaceous nanoparticle, Lennard-Jones potentials

Edited by
Computational Modelling Group
Department of Chemical Engineering and Biotechnology
University of Cambridge
Philippa Fawcett Drive
Cambridge CB3 0AS
United Kingdom

E-Mail: c4e@cam.ac.uk
World Wide Web: https://como.ceb.cam.ac.uk/

Abstract

In this paper we derived the interaction energy between two spherical nanoparticles from the pair-wise Lennard-Jones attractive and repulsive potentials of the constituent atoms of the two particles, and proposed a coagulation efficiency model based on the average particle kinetic energy and the potential well depth (i.e. the minimum interaction energy) between two colliding particles. To test the performance of this new coagulation efficiency model, we applied it in detailed population balance modelling of soot particle size distributions (PSDs), and found better agreement with the measured PSDs in a benchmark premixed ethylene flame than that using the unit coagulation efficiency, especially in the range of small particles with mobility diameter less than 5 nm. Moreover, the agreement between the computed and the measured primary particle size distribution (PPSD) was also improved with the new coagulation efficiency model.

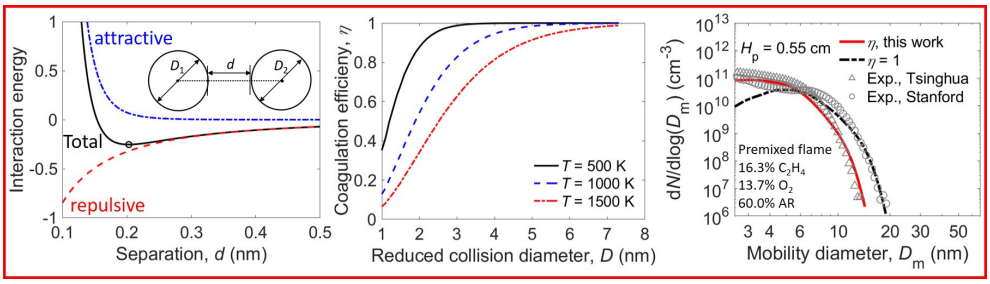

Highlights

- The interaction energy between two spherical particles were derived from the L-J potentials of the constituent atoms of the two particles.
- A coagulation efficiency model for soot was proposed based on the interaction energy between the colliding partners and their kinetic energy.

Contents

1 Introduction

Soot, as one of the byproducts of incomplete combustion of hydrocarbon fuels, is detrimental to both environment and human health [6, 28, 38]. During the past several decades, numerous experimental, theoretical and modelling efforts have been made to gain insights regarding its formation mechanism [1, 3, 9, 10, 13, 21, 25, 32, 33, 42, 43]. Coagulation efficiency η, which measures the sticking probability of two particles upon collisions, has been shown to be a key parameter in soot modelling studies [7, 14, 15, 29, 41]. This parameter may also be named as sticking efficiency in some literature, yet for consistency, only the term coagulation efficiency will be used in this work. For instance, this physical quantity can affect the predicted particle size distributions (PSDs) and primary particle size distributions (PPSDs) significantly according to our recent work on numerical simulations of soot formation in premixed ethylene flames [14, 15]. It was common to assume $\eta = 1$ in soot models [1, 2, 4, 8, 10, 17, 22, 24, 30, 37, 41]. However, when simulating soot formation in a laminar ethylene/air coflow diffusion flame with a discrete sectional model, Zhang et al. [44] found that although soot volume fraction and primary particle size were well produced, the number of primary particles per aggregate was overestimated, which they attributed to the assumption $\eta = 1$ applied in the model. A follow-up work of Zhang et al. [45] recommended $\eta = 20\%$ to well reproduce the experimental data used in [44].

Several experimental studies also indicated that the coagulation efficiency of soot particles should be both size and temperature dependent. D'Alessio et al. [5] found that η decreased drastically with soot particle size decreasing — η of the smallest particles (≈ 3 nm) could decrease to a value near 10^{-3}. In addition, Sirignano and D'Anna [31] reported that η decreased with increasing temperature by comparing the PSDs of soot particles measured at the inlet and the outlet of a flow tube under different temperatures. The physical nature of the coagulation efficiency of nanoparticles was examined by Narsimhan and Ruckenstein [23]. They proposed a model for Brownian coagulation of equal-sized electrically neutral aerosol particles (which was later proved to remain valid also for polydisperse aerosol systems [20]) with van der Waals attraction and Born repulsion taken into account explicitly. In this manner, the coagulation efficiency η of two colliding particles was related to the interaction potentials between them [23]

$$\eta(D_1, D_2) = 1 - \left(1 + \frac{\Phi_0(D_1, D_2)}{k_\mathrm{b} T}\right) \exp\left(-\frac{\Phi_0(D_1, D_2)}{k_\mathrm{b} T}\right), \tag{1}$$

where D_1 and D_2 represent the diameters of two colliding partners, respectively; Φ_0 is the potential well depth, k_b is the Boltzmann constants and T is the temperature. $k_\mathrm{b} T$ measures the average kinetic energy of the nanoparticles. For small particles in the free molecular regime at a typical flame temperature i.e. 1500 – 2000 K, they are very likely to bounce off rather than stick together after a collision due to the relatively high kinetic energy compared with the interaction energy between them, which is called the thermal rebound effect [39].

Based on Eq. (1), D'Alessio et al. [5] proposed a size-dependent coagulation efficiency model for soot, which was employed by Sirignano and D'Anna [31] to simulate the coagulation process of soot particles and by D'Anna and Kent [7] to model soot formation in laminar non-premixed flames. However, the relationship between the interaction energy

and the size of soot particles was not provided explicitly in these studies [5, 7, 31]. Yet according to the reference therein [16], the interaction energy between particles of radii R_1 and R_2 with surface separation d is likely to be calculated through

$$\Phi = -\frac{A}{6}\left(\frac{2R_1R_2}{(2R_1+2R_2+d)d}\right) + \frac{2R_1R_2}{(2R_1+d)(2R_2+d)} + \ln\frac{(2R_1+2R_2+d)d}{(2R_1+d)(2R_2+d)}, \quad (2)$$

where A is the Hamaker constant

$$A = \pi^2\rho_1\rho_2\lambda, \quad (3)$$

ρ_1 and ρ_2 are the atom number density (m^{-3}) of the two particles, respectively; λ is the London dispersion force coefficient [11] (Assume particles are composed of elementary substances). However, the potential well depth Φ_0 cannot be determined using Eq. (2) as Φ decreases monotonically with decreasing separation distance. An assumption that the interaction energy between two colliding partners reaches the minimum at a certain separation distance (for example, 0.4 nm [12]) has to be made. In fact, Eq. (2) only accounts for the attractive potentials between two particles while the repulsive potentials are ignored.

Lindstedt and Waldheim [20] proposed a more complicated coagulation efficiency model for soot by interpolating between the lower limit of η, which was determined by Eq. (1), and the upper limit of η, 1. Nevertheless, the formula used to determine the interaction energy between two particles was not provided in [20]. Besides, mixing functions that require additional empirical parameters such as the coagulation efficiency of pyrene molecules and the critical diameter at which the upper bound began to dominate were introduced to accomplish the interpolation [20].

To establish a coagulation efficiency model based on the framework of Narsimhan and Ruckenstein [23], the potential well depth Φ_0 between two colliding particles has to be determined accurately in the first place, which requires both the attractive and repulsive interaction between two particles to be taken into account when calculating the total interaction energy between them. Since such formula has not been reported in literature, in this work, we will derive the interaction energy between two spherical particles considering both attractive and repulsive potentials. Then a size and temperature dependent coagulation efficiency model for carbonaceous nanoparticles will be proposed based on the potential well depth between colliding partners and the average kinetic energy of the particles. Finally, the performance of this coagulation efficiency model will then be tested by simulating PSDs and PPSDs of soot in premixed ethylene flames with a detailed population balance model.

2 Method

2.1 Potential well depth

Since coagulation efficiency is related to the potential well depth Φ_0, i.e. the minimum interaction energy between two colliding particles, the following part introduces the method used in this work to determine the interaction energy between them.

Each atom in particles is considered to interact pair-wise according to the Lennard-Jones attractive and repulsion potentials

$$U_{ab}(R_{ab}) = 4\varepsilon_{ab}\left(\left(\frac{\sigma_{ab}}{R_{ab}}\right)^{12} - \left(\frac{\sigma_{ab}}{R_{ab}}\right)^{6}\right), \tag{4}$$

where a and b represent two atoms in two particles; ε_{ab} is the potential well depth between two atoms; σ_{ab} is the finite distance at which the inter-atom potential is zero; R_{ab} is the distance between two atoms. Then, the interaction energy Φ between two particles can be given by

$$\Phi = \rho_1\rho_2\int_{V_1}\int_{V_2} U_{ab}(R_{ab})\mathrm{d}V_2\mathrm{d}V_1, \tag{5}$$

where V_1 and V_2 are the volumes of two particles; ρ_1 and ρ_2 are the atom number density of two particles, respectively. Substituting Eq.(4) into Eq.(5) leads to

$$\Phi = \Phi_{\text{attr}} + \Phi_{\text{rep}} = -\rho_1\rho_2\lambda_{ab}\int_{V_1}\int_{V_2}\frac{1}{R_{ab}^6}\mathrm{d}V_2\mathrm{d}V_1 + \rho_1\rho_2\lambda_{ab}\sigma_{ab}^6\int_{V_1}\int_{V_2}\frac{1}{R_{ab}^{12}}\mathrm{d}V_2\mathrm{d}V_1 \tag{6}$$

where

$$\lambda_{ab} = 4\varepsilon_{ab}\sigma_{ab}^6 \tag{7}$$

is the London dispersion force coefficient [11]. The first integration in Eq.(6) represents the attractive interaction energy between two particles, which has been calculated by Hamaker [11] and can be expressed as

$$\Phi_{\text{attr}} = -\frac{1}{12}A\left(\frac{y}{x^2+xy+x} + \frac{y}{x^2+xy+x+y} + 2\ln\frac{x^2+xy+x}{x^2+xy+x+y}\right) \tag{8}$$

where $x = d/(2R_1)$, $y = R_2/R_1$ as shown in Fig. 1. A is the Hamaker constant given by Eq. (3).

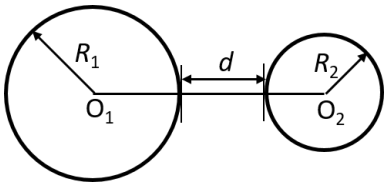

Figure 1: *The schematic diagram of two colliding particles.*

Following the integration techniques used by Hamaker [11], we have calculated the repulsive interaction energy Φ_{rep} between two particles with surface distance d and obtained that

$$\Phi_{\text{rep}} = \frac{1}{37800}A\left(\frac{\sigma_{ab}}{2R_1}\right)^6(\Phi_{\text{rep1}} + \Phi_{\text{rep2}} + \Phi_{\text{rep3}} + \Phi_{\text{rep4}}), \tag{9}$$

$$\Phi_{\text{rep1}} = \frac{2x^2+7y^2+9x+29y+9xy+7}{(1+2x+y)(1+x+y)^7}, \tag{10a}$$

$$\Phi_{\text{rep2}} = \frac{-2x^2-9x+20y+5xy-7}{(1+2x+y)(x+1)^7}, \tag{10b}$$

$$\Phi_{\text{rep3}} = \frac{-2x^2 - 7y^2 + 5x + 20y - 9xy}{(1+2x+y)(x+y)^7}, \tag{10c}$$

$$\Phi_{\text{rep4}} = \frac{2x^2 - 5x + 15y - 5xy}{(1+2x+y)x^7}. \tag{10d}$$

Then the total interaction energy Φ between two particles at a certain distance d can be calculated employing Eq. (6), in which both attractive and repulsive interaction between two spherical bodies are taken into account. As two particles approach, Φ_{attr} decreases while Φ_{rep} increases. Hence, the minimum interaction energy Φ_0 and the corresponding separation distance d_0 can be determined accurately.

2.2 Coagulation efficiency

The coagulation efficiency of two colliding partners is given by Eq. (1), which is applicable for particles in the free molecular regime according to Narsimhan and Ruckenstein [23]. In this work, we will focus on the coagulation of soot particles with mobility diameter $d_{\text{m}} \leq 15\,\text{nm}$, because coagulation efficiency of larger soot particles is close to 1 based on experimental investigation [5]. For 10 nm particles at 1500 K and 1 atm — a typical condition for premixed ethylene flames, the Knudsen number Kn is around 60, which is in the free molecular regime. As Φ_0 between two particles can be determined using equations introduced in Section 2.1, the coagulation efficiency can then be calculated through Eq. (1).

2.3 Detailed population balance modelling for soot

To test the performance of the coagulation efficiency model proposed in this work, we incorporated it into a detailed population balance model (DPBM) and simulated soot formation in premixed ethylene stagnation flames [3, 40]. The DPBM represents soot particles as aggregates composed of overlapping primary particles (PPs), which are in turn composed of a number of polycyclic aromatic hydrocarbons (PAHs). The growth of PAH species within the model is described by a kinetic-Monte-Carlo-aromatic site (KMC-ARS) model [27]. Six particle processes including inception, coagulation, coalescence, condensation, surface growth and sintering are incorporated in the model. A detailed description of the particle model and the stochastic numerical method used to perform population balance simulation can be found in our previous work [14, 18, 19].

3 Results and discussion

3.1 The interaction energy between two spherical particles

Using the equations introduced in Section 2, the dimensionless interaction energy (Φ/A) between two spherical particles of the same size ($D_1 = D_2 = 3\,\text{nm}$) is examined. Assume

particles are composed of C atoms only. σ_{ab} in Eq. (9) is 0.3475 nm according to the L-J parameters for C and C atoms reported by van de Waal [36]. The calculation results are shown in Fig. 2, including the total interaction energy and its two components — attractive potentials and repulsive potentials. The repulsive interaction dominates at a smaller separation between two particles while the attractive interaction dominates at a larger separation. The interaction energy reaches the minimum (marked by the open circle in Fig. 2) at a certain surface separation d_0, as shown by the black solid line. One may notice that the shape of the curve representing the total interaction energy between two spherical bodies is very similar to that of the L-J potentials between two atoms. This is reasonable because the interaction energy between two bodies is actually the sum of the interaction energy between all pairs of atoms in the two bodies. The difference is that after integration of the interaction energy between atoms (see Eq. (4)), the mathematical expression becomes much more complicated (see Eqs. (6),(8),(9),(10a)–(10d)). Theoretically, the analytical solution of d_0, which corresponds to Φ_0, can be obtained if the equation $\frac{\mathrm{d}\Phi}{\mathrm{d}d} = 0$ can be solved. Take the L-J potentials between two atoms as an example. By solving the equation $\frac{\mathrm{d}U_{ab}}{\mathrm{d}R_{ab}} = 0$, the interaction energy reaches the minimum when $R_{ab} = \sqrt[6]{2}\sigma_{ab}$. However, for the interaction between two spherical bodies, the analytical solution becomes difficult to achieve due to the complex mathematical formula; only the numerical solution of d_0 and Φ_0 can be obtained. For the case shown in Fig. 2, the minimum interaction energy Φ_0 is achieved at $d_0 = 0.203\,\mathrm{nm}$.

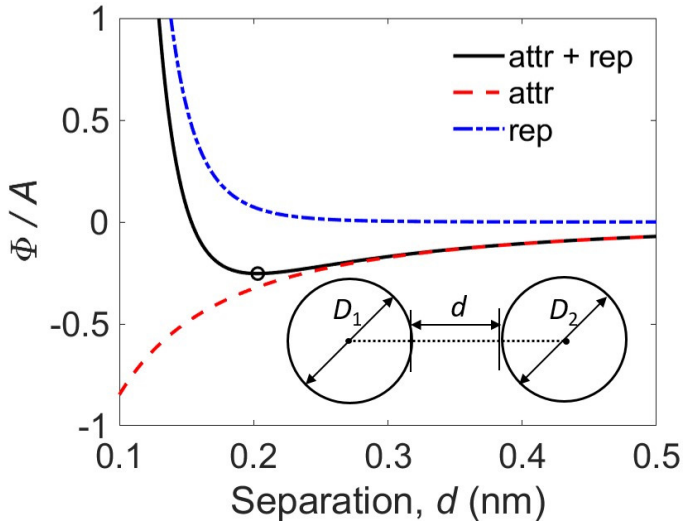

Figure 2: *The dimensionless total, attractive and repulsive interaction energy (Φ/A) between two spherical particles versus the surface separation d between them. ($D_1 = D_2 = 3.0\,\mathrm{nm}$; Particles are composed of C atoms only; $\sigma_{CC} = 0.3475\,\mathrm{nm}$ [36])*

To investigate whether d_0 is sensitive to the size of the colliding particles, the interaction energy of three pairs of particles is examined. As shown in Fig. 3, although the potential well depth Φ_0 between the pair of particles with larger diameters ($D_1 = D_2 = 15\,\mathrm{nm}$) is much deeper than that with small diameters ($D_1 = D_2 = 3\,\mathrm{nm}$), the separation distance

corresponding to the minimum interaction energy, i.e. d_0 is always around 0.2 nm. Fig. 3 also demonstrates that the potential well depth of two colliding particles mainly depends on the smaller one between them, as Φ_0 of two particles with diameters being 3 nm and 15 nm is much closer to Φ_0 of two particles with diameters both being 3 nm.

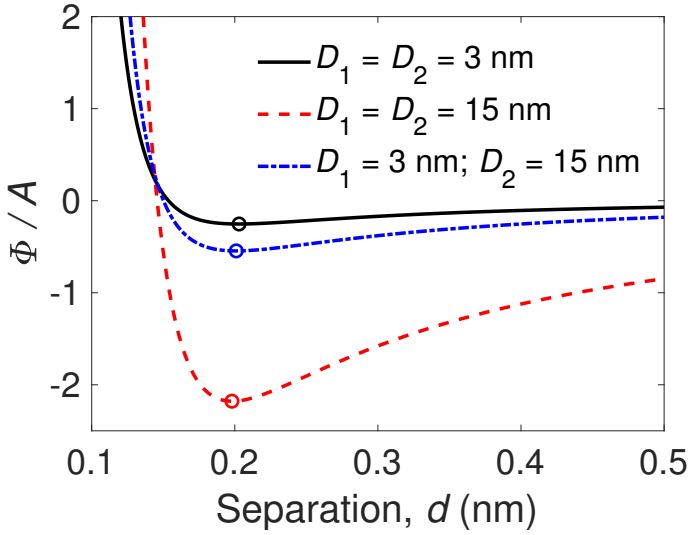

Figure 3: *The dimensionless interaction energy (Φ/A) of three pairs of spherical particles with different diameters. (D_1 and D_2 represent diameters of two colliding particles, respectively; Particles are composed of C atoms only; $\sigma_{CC} = 0.3475$ nm [36])*

3.2 Coagulation efficiency of nascent soot particles

Soot particles are composed of C atoms and H atoms, and therefore the parameters of L-J potentials for C and C atoms, C and H atoms, H and H atoms are required to calculate the interaction energy between two soot particles. In this work, the L-J parameters are taken from Pascazio et al. [26] as listed in Table 1 to describe the interaction energy between soot particles. This is because polycyclic aromatic hydrocarbons (PAHs) are commonly accepted to be major components of soot particles, and the L-J parameters reported in [26] were calculated by fitting the position and depth of the minima of the iso-PAHAP potential [34, 35], which is a well-established potential to describe the intermolecular energy between PAHs and has already been employed in a number of molecular dynamics studies investigating properties of PAH clusters. Besides the parameters of L-J potentials, the number density (m^{-3}) of C and H atoms in soot particles also needs to be determined, which can be estimated based on the mass density of soot particles ρ_{soot} and the C/H ratio. According to a recent experimental work of Wang et al. [40], the mass density of soot particles produced in premixed ethylene stagnation flames is in the range of 600 — 1000 kg/m^3 and the C/H ratio is in the range of 1.7 to 3.7. Since we focus on the coagulation efficiency of small soot particles (< 15 nm), the C/H ratio for soot particles is chosen to be 1.8, which is the C/H ratio for ≈ 10 nm soot particles as reported in [40]. ρ_{soot} is assigned to 700 kg/m^3, which is the mass density of ≈ 10 nm soot particles in

Flame A3 in [40], where the flame condition is very similar to that in the benchmark premixed ethylene stagnation flame. Based on $\rho_{\text{soot}} = 700\,\text{kg/m}^3$ and C/H = 1.8 and with the assumption that both C and H atoms are evenly distributed inside spherical particles, the number density of C and H atoms in soot particles can be estimated as 3.36×10^{28} m^{-3} and 1.86×10^{28} m^{-3}, respectively. The interaction energy between two soot particles

Table 1: *Parameters of the Lennard-Jones potentials used to describe the interaction energy between soot particles.*

Parameter	CC	CH	HH	Ref.
σ_{ab} [nm]	0.3516	0.3029	0.3	[26]
ε_{ab} [kJ mol^{-1}]	0.2599	0.2257	0.0729	

(particle 1 and particle 2) can be obtained through

$$\Phi_{\text{soot}} = \Phi_{\text{CC}} + \Phi_{\text{CH}} + \Phi_{\text{HC}} + \Phi_{\text{HH}}, \tag{11}$$

with Φ_{CC}, Φ_{CH}, Φ_{HC}, Φ_{HH} being the interaction energy between C atoms in particle 1 and C atoms in particle 2, C atoms in particle 1 and H atoms in particle 2, H atoms in particle 1 and C atoms in particle 2, H atoms in particle 1 and H atoms in particle 2, respectively. 1000 uniformly distributed random numbers in the range of 1 — 15 nm were generated as the diameters of particle 1, and in the same way another 1000 random numbers were generated as the diameters of particle 2. Then the potential well depth Φ_0 of these 1000 pairs of particles was calculated. Φ_0 against reduced collision diameters of two colliding particles ($D = D_1 D_2/(D_1 + D_2)$) is shown in Fig. 4. The calculated Φ_0 and the reduced diameter D can be well fitted into a third degree polynomial as

$$\begin{aligned}\Phi_0(D) = &-6.6891 \times 10^{-23} D^3 + 1.1244 \times 10^{-21} D^2 \\ &+ 1.1394 \times 10^{-20} D - 5.5373 \times 10^{-21},\end{aligned} \tag{12}$$

which is shown by the solid line in Fig. 4. For comparison, the average kinetic energy of particles ($\frac{3}{2} k_b T$) at two different temperatures – 500 K and 1500 K are also displayed. It is illustrated in Fig. 4 that for very small particles (< 5 nm), the interaction energy between them is of the same order of the average thermal kinetic energy of the particles or even smaller, especially at a higher temperature. Hence small particles at high temperatures are very likely to rebound rather than stick together upon collisions.

With Φ_0 of two colliding soot particles determined, the coagulation efficiency of soot particles can be calculated using Eq. (1). The resulting coagulation efficiency versus the reduced diameter of two colliding particles at three different temperatures are displayed in Fig. 5. It is clear that coagulation efficiency decreases with decreasing particle size and increasing temperature. Take 1000 K as an example. The coagulation efficiency almost approaches to 1 when the reduced collision diameter is around 5 nm (Note that the reduced collision diameter of two 10 nm particles is 5 nm). This means two particles with diameters both being 10 nm will always stick together after collisions, which is consistent with experimental observations [5]. Since the kinetic energy of particles are greater at higher temperatures, the potential energy between the two particles may not be enough to hold them together, thus causing a much lower coagulation efficiency at 1500 K than that at 500 K.

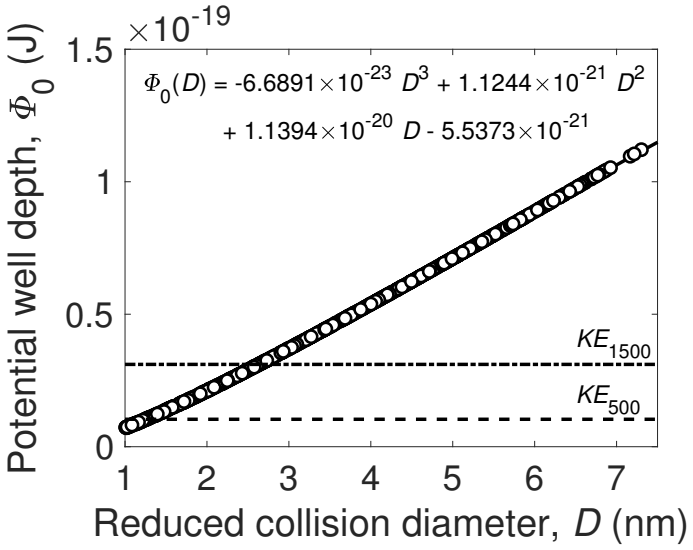

Figure 4: *The potential well depth Φ_0 between two spherical particles against their reduced collision diameters. Black open circles represents the calculated potential well depth between 1000 pairs of particles. The black solid line is the third degree polynomial fitted potential well depth against the reduced collision diameters. KE_{500} and KE_{1500} represent the estimated average kinetic energy of particles at* 500 K *and* 1500 K*, respectively.*

3.3 Simulated soot particle size distributions (PSDs) and primary particle size distributions (PPSDs)

To test the performance of this new size and temperature dependent coagulation efficiency model, we incorporated it into a detailed population balance model for soot [14] and simulated the PSDs of soot in a benchmark premixed ethylene flame (16.3% (mol) C_2H_4, 23.7% O_2, 60.0% AR) [3]. The experimental results in Fig. 6 are reported by two laboratories (Stanford and Tsinghua) measuring soot PSDs in the same benchmark flame with similar sampling probes and mobility measurement techniques [3]. In Fig. 6(a), the experimental PSDs do not agree well with each other for particles larger than 6 nm, while they are consistent when particles are smaller than 5 nm. The computed PSDs of soot at two stagnation plate heights ($H_p = 0.55, 1.2$ cm) employing η proposed in this work and $\eta = 1$ are also shown in Fig. 6. With the new coagulation efficiency model, the predicted PSD in Fig. 6(a) agrees better with the measured results in small particle region, especially for those particles < 5 nm. For particles > 6 nm, the computed PSDs using both η lie within the uncertainties of experimental measurements. As for particles larger than 20 nm, the predicted PSD by the new model is very close to that by the unit coagulation efficiency model as shown in Fig. 6(b), because the coagulation efficiency of large particles in the new model is also almost 1.

It is also noteworthy that the computed PSD at $H_p = 1.2$ cm still differed from the measured one for particles < 3 nm as shown in Fig. 6(b). This discrepancy may be attributed to both experimental uncertainties for measuring such small particles and some model assumptions. First, particles < 3 nm are freshly nucleated soot particles. However, the

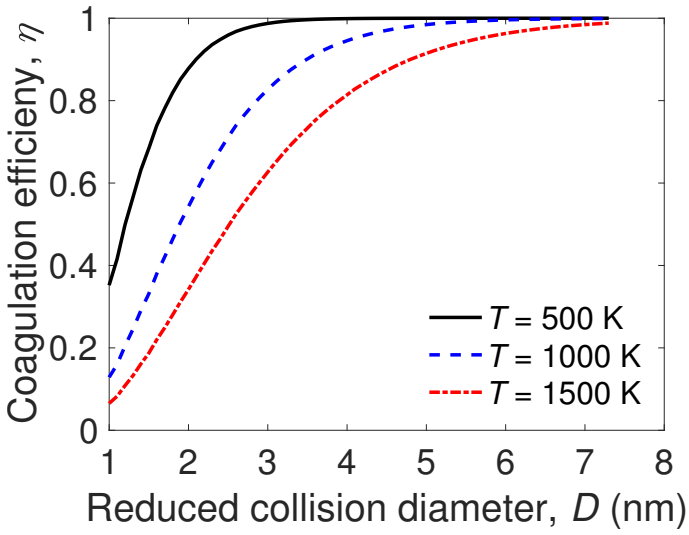

Figure 5: *Coagulation efficiency versus reduced diameter of two colliding particles at T = 500, 1000 and* 1500 K.

nucleation mechanism for soot particles still remains unclear. In the detailed population balance model used in this work, the nucleation process is described as two PAH molecules sticking together after collisions, while how nucleation actually proceeds in flames is unclear and may be much more complicated than the current assumption applied in the model. Second, we derived the interaction energy for spherical particles, however, the shape of very small soot particles can deviate from spherical, if we consider freshly nucleated soot particles composing of only a small number of planar PAHs. This indicates further study on the coagulation process of very small particles which may be non-spherical in shape is required. Molecular dynamics simulation can be helpful to investigate the influence of the spherical particle assumption in future work.

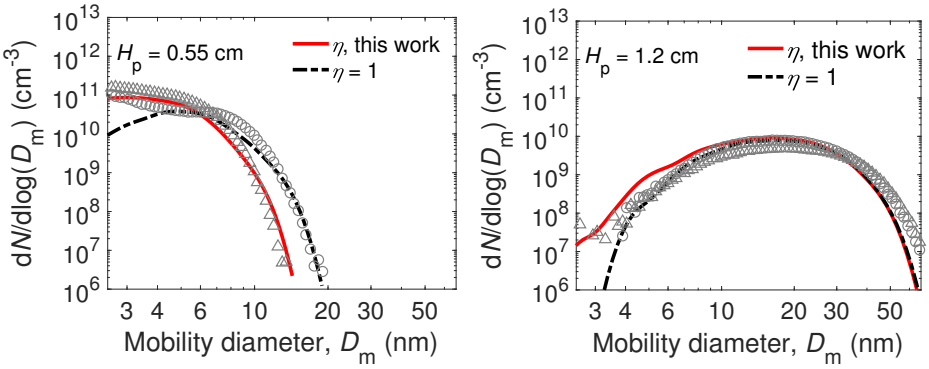

(a) (b)

Figure 6: *The computed PSDs (Lines) in the benchmark premixed ethylene stagnation flames with two stagnation plate heights (H_p) [3] using coagulation efficiency $\eta = 1$ and the coagulation efficiency model proposed in this work. (a) $H_p =$* 0.55 cm*; (b) $H_p =$* 1.2 cm*. Symbols are experimental results reported by Stanford (circles) and Tsinghua (triangles) in [3].*

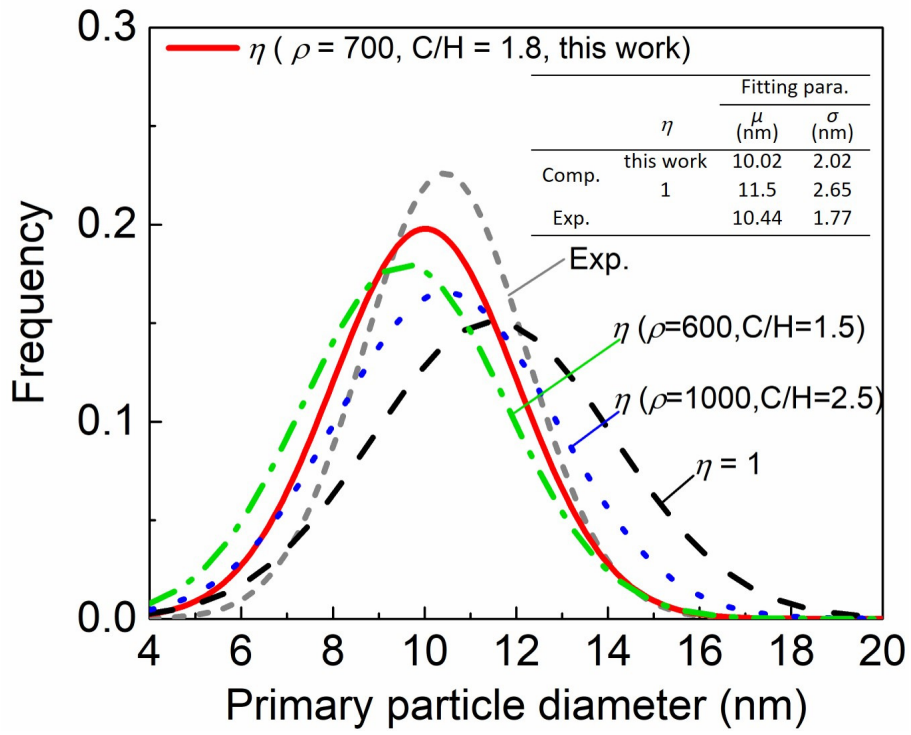

Figure 7: *Computed and experimentally measured PPSDs (fitted normal distributions) of soot in a C_2H_4 premixed flame in [40] at stagnation plate height $H_p = 1.2\,\mathrm{cm}$. (Unit of mass density ρ: $\mathrm{kg/m^3}$)*

In addition to PSDs, we also examined the performance of this new coagulation efficiency model on predicting the primary particle size distribution (PPSD) of soot in a premixed C_2H_4 stagnation flame (16% (mol) C_2H_4, 24.0% O_2, 60.0% AR; see Flame A3 in [40]). Wang et al. [40] obtained the PPSD by processing the observed transmission electron microscopy (TEM) images and measuring the primary particle size. Normal distributions fitted to the computed and the measured PPSDs are shown in Fig. 7. With η proposed in this work, the computed PPSD which is represented by the red solid line, agrees reasonably well with the experimental measurements. However, the primary particle size is overestimated with $\eta = 1$. This is because higher η increases the probability of small particles sticking together, and if the diameter of a primary particle is smaller than d_{crit} (a parameter defined in the detailed population balance soot model [14, 15]), it will instantaneously merge with its neighboring primary particles, thus leading to a larger primary particle. Besides the computed PPSDs with η proposed in this work, the calculated PPSDs with η based on another two sets of parameters are also displayed ($\rho = 600\,\mathrm{kg/m^3}, \mathrm{C/H} = 1.5$ and $\rho = 1000\,\mathrm{kg/m^3}, \mathrm{C/H} = 2.5$), which will be discussed in detail in the parametric sensitivity analysis in Section 3.4.

3.4 Parametric sensitivity analysis

In this work, the coagulation efficiency model for soot is proposed based on the potential well depth Φ_0 of two colliding soot particles and the average kinetic energy of the par-

ticles. Φ_0 depends on composition of soot particles. The Hamaker constant A, which is required when calculating both the attractive (see Eq. (8)) and the repulsive interaction (see Eq. (9)) between two particles, depends on the number density of C and H atoms of soot (see Eq. (3)) and can be calculated through

$$A_{\text{soot}} = \pi^2 \rho_{\text{C}}^2 \lambda_{\text{C}} + \pi^2 \rho_{\text{H}}^2 \lambda_{\text{H}} + 2\pi^2 \rho_{\text{C}} \rho_{\text{H}} \lambda_{\text{CH}}, \tag{13}$$

where

$$\lambda_{\text{C}} = 4\varepsilon_{\text{CC}} \sigma_{\text{CC}}^6, \tag{14}$$

$$\lambda_{\text{H}} = 4\varepsilon_{\text{HH}} \sigma_{\text{HH}}^6, \tag{15}$$

$$\lambda_{\text{CH}} = 4\varepsilon_{\text{CH}} \sigma_{\text{CH}}^6, \tag{16}$$

with the L-J parameters being listed in Table 1. The number density of C and H atoms — ρ_{C} and ρ_{H} can be determined based the mass density ρ_{soot} and C/H ratio of soot particles. In Section 3.2, we assumed the soot density $\rho = 700\,\text{kg/m}^3$ and C/H ratio = 1.8 (which corresponds to $A = 5.2 \times 10^{-20}\,\text{J}$) based on the experimental results on nascent soot particles in premixed ethylene flames [40]. However, for nascent soot particles with diameter $\leq 15\,\text{nm}$, ρ_{soot} was in the range from 600 to $1000\,\text{kg/m}^3$ and C/H ratio could vary in the range from 1.7 to 2.5 [40]. ρ_{soot} and C/H ratio of soot particles keep changing because their constituents and internal spatial structure keep evolving with residence time in flames. Although based on the current choice of soot density ρ and C/H ratio, a coagulation efficiency model was proposed and better agreement between the computed and measured results for both PSDs and PPSDs was obtained, it is still necessary to investigate the effect of the choice of ρ and C/H ratio on the coagulation efficiency model. Generally speaking, a low C/H ratio of soot particles should correspond to a low mass density. Therefore, we chose another two sets of parameters – $\rho = 600\,\text{kg/m}^3, \text{C/H} = 1.5$ (which corresponds to $A = 4.0 \times 10^{-20}\,\text{J}$) and $\rho = 1000\,\text{kg/m}^3, \text{C/H} = 2.5$ (which corresponds to $A = 9.9 \times 10^{-20}\,\text{J}$) to calculate the potential well depth and the resulting coagulation efficiency. As illustrated in Fig. 8, larger mass density ρ_{soot} and C/H ratio lead to deeper potential well depth between colliding partners, thus η is higher. This indicates that the choice of ρ and C/H ratio can affect η. Figure 7 shows influence of these two parameters on the computed PPSDs. The computational results shown in Fig. 7 are encouraging because they suggest that although uncertainties exist in ρ and C/H ratio, the predicted PPSDs always agree better with the measured results when a size and temperature dependent η is employed. Figure 7 also illustrates that among the three parameter sets for determining η, $\rho = 700\,\text{kg/m}^3, \text{C/H} = 1.8$ leads to the best agreement with the experimental result. This is reasonable because $\rho = 700\,\text{kg/m}^3$ and C/H = 1.8 may represent the average properties of soot. It is worth mentioning that in previous modelling work, Hamaker constant A of soot has been assigned different values, such as $1 \times 10^{-20}\,\text{J}$ and $2 \times 10^{-20}\,\text{J}$ [31], $3 \times 10^{-20}\,\text{J}$ [5], $5 \times 10^{-20}\,\text{J}$ [7] and $7 \times 10^{-20}\,\text{J}$ [20] to model the coagulation process of soot particles. Here we suggest that when modelling the coagulation process of soot in a certain flame, the Hamaker constant A should be assigned based on the properties of soot particles generated under similar flame condition.

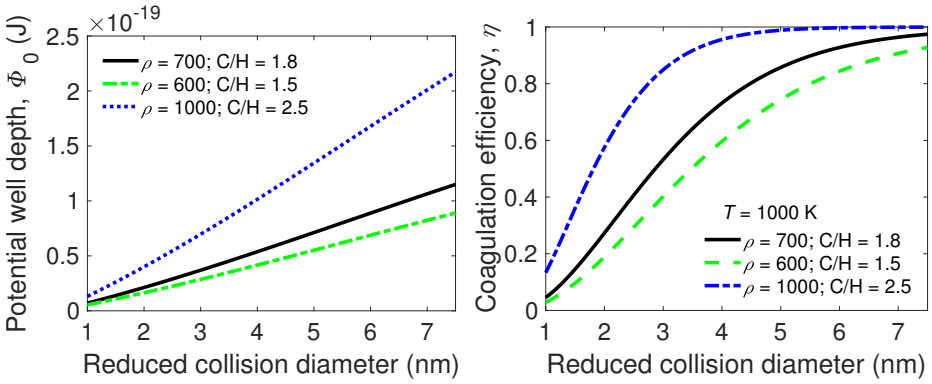

Figure 8: *Potential well depth (a) and Coagulation efficiency at* 1000 K *(b) versus reduced collision diameter of two colliding particles with different mass densities and C/H ratios of soot particles. (Unit of mass density* ρ*:* $\mathrm{kg/m^3}$*)*

4 Conclusion

In this work, we derived the interaction energy between two spherical nanoparticles from the pair-wise Lennard-Jones attractive and repulsive potentials of the constituent atoms of the two particles and proposed a coagulation efficiency model based on the average particle kinetic energy and the potential well depth (i.e. the minimum interaction energy) between two colliding particles. To test the performance of this new size and temperature dependent coagulation efficiency model, we implemented it in a detailed population balance model for soot and simulated soot particle size distributions (PSDs) in a benchmark premixed ethylene flame. Compared with the unit coagulation efficiency, better agreement between the computed PSDs and the measured PSDs was achieved with this new coagulation efficiency model, especially for particles < 5 nm. Moreover, the agreement between the computed and the measured primary particle size distribution (PPSD) was also improved with the new coagulation efficiency model.

It is worth mentioning that although in this work we studied the interaction energy between carbonaceous nanoparticles, the derived formula of interaction energy between two spherical particles in this work can be applied to other kinds of particles, as long as the atomic pairwise interaction can be described by the Lennard-Jones attractive and repulsive potentials. In this manner, the potential well depth between two spherical particles can be determined accurately.

Acknowledgements

This project is supported by the National Science Foundation of China (51761125012). Markus Kraft and Casper Lindberg have been supported by the National Research Foundation (NRF), Prime Minister's Office, Singapore under its Campus for Research Excellence and Technological Enterprise(CREATE) programme. Markus Kraft acknowledges

the support of the Alexander von Humboldt foundation.

References

[1] J. Appel, H. Bockhorn, and M. Frenklach. Kinetic modeling of soot formation with detailed chemistry and physics: laminar premixed flames of C_2 hydrocarbons. *Combustion and Flame*, 121:122 – 136, 2000. doi:10.1016/S0010-2180(99)00135-2.

[2] M. Balthasar and M. Kraft. A stochastic approach to calculate the particle size distribution function of soot particles in laminar premixed flames. *Combustion and Flame*, 133:289 – 298, 2003. doi:10.1016/S0010-2180(03)00003-8.

[3] J. Camacho, C. Liu, C. Gu, H. Lin, Z. Huang, Q. Tang, X. You, C. Saggese, Y. Li, H. Jung, L. Deng, I. Wlokas, and H. Wang. Mobility size and mass of nascent soot particles in a benchmark premixed ethylene flame. *Combustion and Flame*, 162: 3810 – 3822, 2015. doi:10.1016/j.combustflame.2015.07.018.

[4] D. Chen, Z. Zainuddin, E. K. Y. Yapp, J. Akroyd, S. Mosbach, and M. Kraft. A fully coupled simulation of PAH and soot growth with a population balance model. *Proceedings of the Combustion Institute*, 34:1827 – 1835, 2013. doi:10.1016/j.proci.2012.06.089.

[5] A. D'Alessio, A. Barone, R. Cau, A. D'Anna, and P. Minutolo. Surface deposition and coagulation efficiency of combustion generated nanoparticles in the size range from 1 to 10 nm. *Proceedings of the Combustion Institute*, 30:2595 – 2603, 2005. doi:10.1016/j.proci.2004.08.267.

[6] A. D'Anna. Combustion-formed nanoparticles. *Proceedings of the Combustion Institute*, 32:593 – 613, 2009. doi:10.1016/j.proci.2008.09.005.

[7] A. D'Anna and J. Kent. A model of particulate and species formation applied to laminar, nonpremixed flames for three aliphatic-hydrocarbon fuels. *Combustion and Flame*, 152:573 – 587, 2008. doi:10.1016/j.combustflame.2007.08.003.

[8] M. Frenklach. Method of moments with interpolative closure. *Chemical Engineering Science*, 57:2229 – 2239, 2002. doi:10.1016/S0009-2509(02)00113-6.

[9] M. Frenklach. Reaction mechanism of soot formation in flames. *Physical Chemistry Chemical Physics*, 4:2028–2037, 2002. doi:10.1039/B110045A.

[10] M. Frenklach and H. Wang. Detailed modeling of soot particle nucleation and growth. *Symposium (International) on Combustion*, 23:1559 – 1566, 1991. doi:10.1016/S0082-0784(06)80426-1.

[11] H. Hamaker. The London-van der Waals attraction between spherical particles. *Physica*, 4:1058 – 1072, 1937. doi:10.1016/S0031-8914(37)80203-7.

[12] W. C. Hinds. *Aerosol technology: properties, behavior, and measurement of airborne particles*. John Wiley & Sons, New York, second edition, 1999.

[13] D. Hou and X. You. Reaction kinetics of hydrogen abstraction from polycyclic aromatic hydrocarbons by H atoms. *Physical Chemistry Chemical Physics*, 19:30772–30780, 2017.

[14] D. Hou, C. S. Lindberg, M. Y. Manuputty, X. You, and M. Kraft. Modelling soot formation in a benchmark ethylene stagnation flame with a new detailed population balance model. *Combustion and Flame*, 203:56 – 71, 2019. doi:10.1016/j.combustflame.2019.01.035.

[15] D. Hou, C. S. Lindberg, M. Wang, M. Y. Manuputty, X. You, and M. Kraft. Simulation of soot particle morphology in a premixed ethylene stagnation flame, 2019. Submitted for publication.

[16] J. N. Israelachvili. *Intermolecular and surface forces*. Academic press, third edition, 2011.

[17] A. Kazakov and M. Frenklach. Dynamic Modeling of Soot Particle Coagulation and Aggregation: Implementation With the Method of Moments and Application to High-Pressure Laminar Premixed Flames. *Combustion and Flame*, 114:484 – 501, 1998. doi:10.1016/S0010-2180(97)00322-2.

[18] C. S. Lindberg, M. Y. Manuputty, J. Akroyd, and M. Kraft. A two-step simulation methodology for modelling stagnation flame synthesised aggregate nanoparticles. *Combustion and Flame*, 202:143 – 153, 2019. doi:10.1016/j.combustflame.2019.01.010.

[19] C. S. Lindberg, M. Y. Manuputty, E. K. Yapp, J. Akroyd, R. Xu, and M. Kraft. A detailed particle model for polydisperse aggregate particles. *Journal of Computational Physics*, 2019. doi:10.1016/j.jcp.2019.06.074.

[20] R. Lindstedt and B. Waldheim. Modeling of soot particle size distributions in premixed stagnation flow flames. *Proceedings of the Combustion Institute*, 34:1861 – 1868, 2013. doi:10.1016/j.proci.2012.05.047.

[21] J. Mei, M. Wang, X. You, and C. K. Law. Quantitative measurement of particle size distributions of carbonaceous nanoparticles during ethylene pyrolysis in a laminar flow reactor. *Combustion and Flame*, 200:15 – 22, 2019. doi:10.1016/j.combustflame.2018.11.010.

[22] N. Morgan, M. Kraft, M. Balthasar, D. Wong, M. Frenklach, and P. Mitchell. Numerical simulations of soot aggregation in premixed laminar flames. *Proceedings of the Combustion Institute*, 31:693 – 700, 2007. doi:10.1016/j.proci.2006.08.021.

[23] G. Narsimhan and E. Ruckenstein. The Brownian coagulation of aerosols over the entire range of Knudsen numbers: Connection between the sticking probability and the interaction forces. *Journal of Colloid and Interface Science*, 104:344 – 369, 1985. doi:10.1016/0021-9797(85)90044-X.

[24] A. Naseri, A. Veshkini, and M. J. Thomson. Detailed modeling of CO_2 addition effects on the evolution of soot particle size distribution functions in premixed laminar ethylene flames. *Combustion and Flame*, 183:75 – 87, 2017. doi:10.1016/j.combustflame.2017.04.028.

[25] B. Öktem, M. P. Tolocka, B. Zhao, H. Wang, and M. V. Johnston. Chemical species associated with the early stage of soot growth in a laminar premixed ethylene-oxygen-argon flame. *Combustion and Flame*, 142:364 – 373, 2005. doi:10.1016/j.combustflame.2005.03.016.

[26] L. Pascazio, M. Sirignano, and A. D'Anna. Simulating the morphology of clusters of polycyclic aromatic hydrocarbons: The influence of the intermolecular potential. *Combustion and Flame*, 185:53 – 62, 2017. doi:10.1016/j.combustflame.2017.07.003.

[27] A. Raj, M. Celnik, R. Shirley, M. Sander, R. Patterson, R. West, and M. Kraft. A statistical approach to develop a detailed soot growth model using PAH characteristics. *Combustion and Flame*, 156:896 – 913, 2009. doi:10.1016/j.combustflame.2009.01.005.

[28] H. Richter and J. Howard. Formation of polycyclic aromatic hydrocarbons and their growth to soot – a review of chemical reaction pathways. *Progress in Energy and Combustion Science*, 26:565 – 608, 2000. doi:10.1016/S0360-1285(00)00009-5.

[29] C. Saggese, S. Ferrario, J. Camacho, A. Cuoci, A. Frassoldati, E. Ranzi, H. Wang, and T. Faravelli. Kinetic modeling of particle size distribution of soot in a premixed burner-stabilized stagnation ethylene flame. *Combustion and Flame*, 162:3356 – 3369, 2015. doi:10.1016/j.combustflame.2015.06.002.

[30] M. Sander, R. I. Patterson, A. Braumann, A. Raj, and M. Kraft. Developing the PAH-PP soot particle model using process informatics and uncertainty propagation. *Proceedings of the Combustion Institute*, 33:675 – 683, 2011. doi:10.1016/j.proci.2010.06.156.

[31] M. Sirignano and A. D'Anna. Coagulation of combustion generated nanoparticles in low and intermediate temperature regimes: An experimental study. *Proceedings of the Combustion Institute*, 34:1877 – 1884, 2013. doi:10.1016/j.proci.2012.06.119.

[32] Q. Tang, J. Mei, and X. You. Effects of CO_2 addition on the evolution of particle size distribution functions in premixed ethylene flame. *Combustion and Flame*, 165: 424 – 432, 2016. doi:10.1016/j.combustflame.2015.12.026.

[33] Q. Tang, R. Cai, X. You, and J. Jiang. Nascent soot particle size distributions down to 1 nm from a laminar premixed burner-stabilized stagnation ethylene flame. *Proceedings of the Combustion Institute*, 36:993 – 1000, 2017. doi:10.1016/j.proci.2016.08.085.

[34] T. S. Totton, A. J. Misquitta, and M. Kraft. A first principles development of a general anisotropic potential for polycyclic aromatic hydrocarbons. *Journal of Chemical Theory and Computation*, 6:683–695, 2010. doi:10.1021/ct9004883.

[35] T. S. Totton, A. J. Misquitta, and M. Kraft. A quantitative study of the clustering of polycyclic aromatic hydrocarbons at high temperatures. *Physical Chemistry Chemical Physics*, 14:4081–4094, 2012. doi:10.1039/C2CP23008A.

[36] B. W. van de Waal. Calculated ground-state structures of 13-molecule clusters of carbon dioxide, methane, benzene, cyclohexane, and naphthalene. *The Journal of Chemical Physics*, 79:3948–3961, 1983. doi:10.1063/1.446263.

[37] A. Veshkini, N. A. Eaves, S. B. Dworkin, and M. J. Thomson. Application of PAH-condensation reversibility in modeling soot growth in laminar premixed and nonpremixed flames. *Combustion and Flame*, 167:335 – 352, 2016. doi:10.1016/j.combustflame.2016.02.024.

[38] H. Wang. Formation of nascent soot and other condensed-phase materials in flames. *Proceedings of the Combustion Institute*, 33:41 – 67, 2011. doi:10.1016/j.proci.2010.09.009.

[39] H.-C. Wang and G. Kasper. Filtration efficiency of nanometer-size aerosol particles. *Journal of Aerosol Science*, 22:31 – 41, 1991. doi:10.1016/0021-8502(91)90091-U.

[40] M. Wang, Q. Tang, J. Mei, and X. You. On the effective density of soot particles in premixed ethylene flames. *Combustion and Flame*, 198:428 – 435, 2018. doi:10.1016/j.combustflame.2018.10.004.

[41] E. K. Y. Yapp, D. Chen, J. Akroyd, S. Mosbach, M. Kraft, J. Camacho, and H. Wang. Numerical simulation and parametric sensitivity study of particle size distributions in a burner-stabilised stagnation flame. *Combustion and Flame*, 162:2569 – 2581, 2015. doi:10.1016/j.combustflame.2015.03.006.

[42] H.-B. Zhang, X. You, H. Wang, and C. K. Law. Dimerization of polycyclic aromatic hydrocarbons in soot nucleation. *The Journal of Physical Chemistry A*, 118:1287–1292, 2014. doi:10.1021/jp411806q.

[43] H.-B. Zhang, D. Hou, C. K. Law, and X. You. Role of carbon-addition and hydrogen-migration reactions in soot surface growth. *The Journal of Physical Chemistry A*, 120:683–689, 2016. doi:10.1021/acs.jpca.5b10306.

[44] Q. Zhang, H. Guo, F. Liu, G. Smallwood, and M. Thomson. Modeling of soot aggregate formation and size distribution in a laminar ethylene/air coflow diffusion flame with detailed PAH chemistry and an advanced sectional aerosol dynamics model. *Proceedings of the Combustion Institute*, 32:761 – 768, 2009. doi:10.1016/j.proci.2008.06.109.

[45] Q. Zhang, M. Thomson, H. Guo, F. Liu, and G. Smallwood. A numerical study of soot aggregate formation in a laminar coflow diffusion flame. *Combustion and Flame*, 156:697 – 705, 2009. doi:10.1016/j.combustflame.2008.10.022.